Journal of Physics D: Applied Physics

PAPER

Investigating the impact of catalysts on N_2 rotational and vibrational temperatures in low pressure plasmas

To cite this article: Angela R Hanna *et al* 2019 *J. Phys. D: Appl. Phys.* **52** 345202

IOP Publishing Journal of Physics D: Applied Physics

J. Phys. D: Appl. Phys. **52** (2019) 345202 (13pp) https://doi.org/10.1088/1361-6463/ab2291

Investigating the impact of catalysts on N_2 rotational and vibrational temperatures in low pressure plasmas

Angela R Hanna, Tara L Van Surksum and Ellen R Fisher[1]

Department of Chemistry, Colorado State University, Fort Collins, CO 80524-1872, United States of America

E-mail Ellen.Fisher@colostate.edu

Received 25 February 2019, revised 1 May 2019
Accepted for publication 17 May 2019
Published 24 June 2019

Abstract

Future application of plasma assisted catalysis (PAC) requires a thorough understanding of energy partitioning within the plasma-catalyst system. We have studied the impact of adding a catalyst (TiO_2 and zeolites) on the plasma energetics within an N_2 low-temperature, radio frequency (RF) plasma by measuring the vibrational and rotational temperatures of the gas-phase N_2. The presence of either micro- or nano-structured materials (zeolite and TiO_2 substrates, respectively) within the plasma significantly decreases N_2 (g) vibrational temperature, suggesting these materials promote vibrational relaxation within the discharge upon interaction with a catalytic substrate. In addition to evaluating the spectroscopic characteristics of the N_2 discharge, we have assessed material morphology and chemical composition before and after plasma exposure. The porous network of both TiO_2 and zeolite substrates were maintained after plasma exposure, although small amounts of nitrogen incorporation occurred at the surface of both materials.

Keywords: plasma assisted catalysis, vibrational temperature, rotational temperature, energy partitioning, optical emission spectroscopy

S Supplementary material for this article is available online

(Some figures may appear in colour only in the online journal)

Introduction

Plasma assisted catalysis (PAC) generally describes the combining of a plasma system with a catalytic material for enhanced decomposition of a waste stream. PAC has recently received much attention within the plasma community because the non-thermal nature of the plasmas employed allows access to processes energetically unavailable under thermal conditions and because of the enormous potential to increase feed gas conversion [1–4]. PAC can be widely applied across a wide range of disciplines and applications, including treatment of waste gases [5, 6]; CO_2 capture and conversion to high-value materials [7, 8]; methane reforming [9, 10]; ammonia synthesis [11]; and fabrication of carbon nanostructures and supported nanocatalysts via non-thermal plasma methods [12, 13]. Regardless of end application, the fundamental scientific questions and challenges that must be addressed before implementation of PAC as a viable technology are remarkably similar, such as optimized reactor and catalyst design. Indeed, paramount to the future of PAC development are a number of essential pieces, such as understanding of plasma generation and general operating conditions; the selection of catalysts, where both chemical and physical properties need to be considered; and the elucidation of interactions between plasma and material [14, 15].

In single-stage PAC systems, the catalyst is placed directly in the discharge, allowing all plasma species to interact with the surface of the catalyst. The resulting range of dissociation products can lead to a complex and entangled chemistry within the plasma system. Although it is generally understood

[1] Author to whom any correspondence should be addressed.

Table 1. Summary of T_V & T_R measurements in N_2 glow discharges.

Source	p (Torr)	P (W)	T_R (K)	T_V (K)	Ref
RF	1	1000	600	—	Porter [50]
DC	0.1–2	*n/a* ($I = 50$ mA)	—	2500–3000, 7200	Cernogora [51]
DBD	0.15	*n/a* ($U = 800$ V)	480	—	Zhang [52]
C-DBD	200–600	25–60	360	2270–3030	Masoud [53]
IPC-RF	—	—	370/470	5000–12000	Britun [54]
RGA	—	—	2200–2500	3200–3700	Gangoli [55]
RGA	atm.	*n/a* ($U = 7$–10 kV)	1160–1508	4874–5105	Wu [32]
DBD	atm.	140	350–575	2200–2500	Yang [56]
ICP-RF	0.05–0.2	50–200	300–500	2000–7000	Hanna [33]
GAP	atm.	*n/a* ($I = 230$ mA)	5500	—	Groger [57]

that catalyst particle size can influence the overall rate and efficiency of PAC processes [2, 3], little is understood about how low-temperature plasmas (LTPs) interact with micro- and nano-structured materials. Furthermore, most studies to date have primarily explored optimizing PAC systems from the standpoint of how well the plasma removes a pollutant [3, 16] or how the plasma affects the material [1, 17–19], with fewer focusing on how the material affects the gas-phase chemistry, energy partitioning within the plasma, or interactions between the plasma and the surface. Energy distributions within non-thermal plasmas typically follow the relationship wherein vibrational temperatures are greater than rotational or gas temperatures, and higher energy electrons and ions play a crucial role in the overall plasma character.

As the precursor gas becomes more complex, these interactions between gas-phase species and catalysts will undoubtedly also become more convoluted and potential synergisms may be difficult to deconstruct. Hence, in this study we examined nitrogen plasmas, a relatively inert, homonuclear, diatomic system that somewhat diminishes the complexity by at least limiting the number and type of gas-phase species that can be formed. Moreover, as evidenced by the selected works listed in table 1, N_2 plasmas have been extensively studied in the literature over decades. Table 1 demonstrates the wide range of N_2 plasma operating conditions, including source ignition, pressure regimes, and power (or charge), and consequently a wide range of rotational and vibrational temperatures (T_R and T_V, respectively) have been documented. Although not an exhaustive list, table 1 studies all examined gas-phase characteristics of N_2 plasmas, without the complexity of adding a catalyst.

Two additional studies that examined internal temperatures of N_2 plasma species in model PAC systems measured T_V and T_R of N_2 utilizing TiO_2 in a packed bed atmospheric dielectric barrier discharge (DBD) system (system pressure (p) of ~101 Pa) [20] and Co-ZSM-5 in a radio frequency (RF) plasma, operated near atmospheric pressure ($p = 90$ Pa) [21]. Tu *et al* found that T_V (N_2) increased dramatically from ~2300–2800 K to ~3200–4100 K when TiO_2 pellets were placed in the plasma and attributed this to an increase in electron temperature (T_e) as a result of the catalyst [20]. Interestingly, the TiO_2 catalyst had no effect on T_R (N_2) at the lowest applied discharge power (P) of 40 W and removed all the positive linear dependence of T_R (N_2) on P observed without TiO_2 ($P = 40$–70 W). Although Tu *et al* noted some of these changes may indicate heating of the substrate, although the true origin of these effects remains unclear. Niu *et al* observed differences in T_V and T_R when employing Co-ZSM-5 as a catalyst [21]. Here, however, T_V (N_2) was ~3100–3400 K *with* the catalyst, more than 1000 K lower than that measured without the Co-ZSM-5 (~4300–5000 K). Although a slight decrease was observed as a function of RF power with the catalyst, the opposite trend was observed without the catalyst. In addition, T_R (N_2) ranged from ~375 K at the lowest P to ~500 K at the highest P, with very little difference between values measured with and without the catalyst. Notably, all of the measurements made in this study were made at $P = 5$–25 W, discharge powers considerably lower than the lowest used by Tu *et al* [20]. Although no explanation was provided for the differences between these internal temperature values and those measured by Tu *et al*, variations in P and the catalyst type could account for the observed dissimilarities.

When nano-structured or porous materials are placed in plasma discharges, spatial inhomogeneity can be created (i.e. microplasmas within pores, localized electric fields) which alters the electrical characteristics of the plasma [22]. Significant experimental and theoretical efforts have explored the formation of microdischarges in different catalytic pores in recent years. Zhang *et al* simulated micro-and nano-sized catalyst pores with a 2D particle-in-cell/Monte Carlo collisional model, demonstrating the formation of microdischarges in both μm-and nm-sized pores; electron density and electron impact ionization rate drastically increase when the plasma stream permeates in the micrometer pore [23]. Likewise, Gu *et al* computationally demonstrated that the discharge is more enhanced on the surface of porous catalysts compared to inside the pores [24]. Clearly, plasma-material synergisms arise from the introduction of a catalyst in a discharge, where the chemical identity and pore size, position in reactor, and amount of catalyst in the discharge are important variables to consider and study. Tu and Whitehead demonstrated different packing methods with Ni/γ-Al_2O_3 catalysts in DBD reactor systems impact the dry reforming of CH_4 [9]. In a fully packed-bed reactor, the authors found a decrease in conversions of CH_4 and CO_2 compared to the system with no catalyst present. When the Ni/γ-Al_2O_3 catalyst particles are partially packed in the discharge, the conversion rate of CH_4 increased to 38% compared to the 30% conversion of the no catalyst system. The authors concluded that the manner

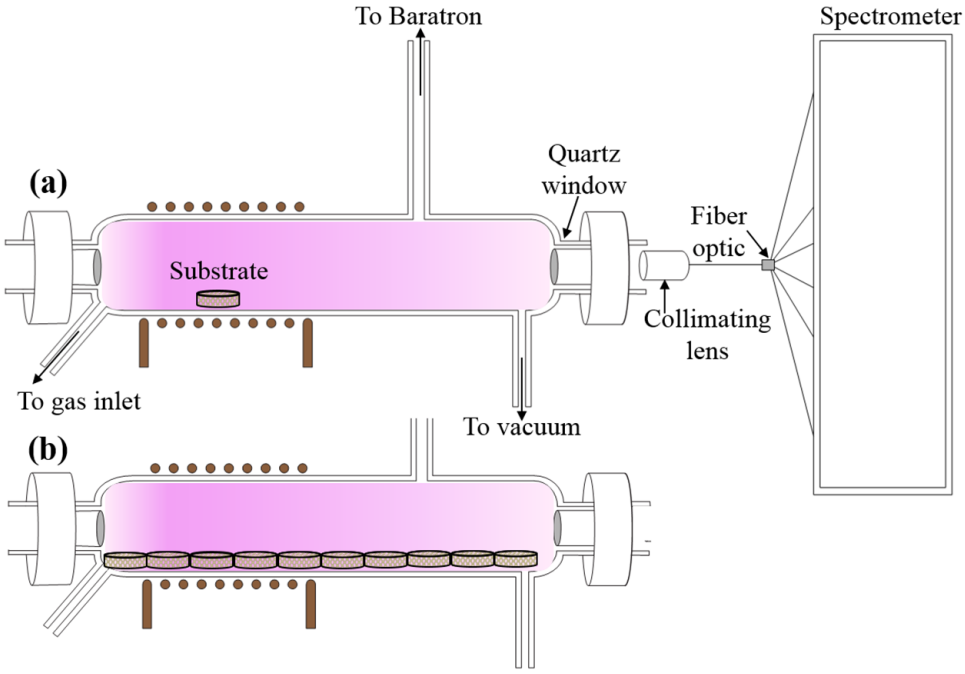

Figure 1. Schematic representation of OES apparatus for low-temperature, ICP systems detailing (a) single substrate placement in the coil region and (b) multiple zeolite substrates in the reactor.

of catalyst packing in a discharge plays an important role in single-stage PAC systems [9].

Here, we further explore all these phenomena by examining the effects of adding catalysts to an N_2 inductively coupled plasma (ICP) operated at relatively low pressure (~50–150 mTorr or ~7–20 Pa). The two catalysts employed here are TiO_2 nanoparticles (for direct comparison to the results of Tu *et al*) and micro-structured NaY zeolite (Si/Al ratio of 3.5 ± 0.2). T_V (N_2) and T_R (N_2) were measured as a function of P and p using optical emission spectroscopy (OES). We have also examined the morphology and chemical composition of the catalysts using scanning electron microscopy (SEM) and x-ray photoelectron spectroscopy (XPS) both before and after plasma exposure to determine the impact of the plasma on the materials. To further probe the impact of catalyst packing on the synergisms between the plasma and catalysts, we have studied single-substrate systems, where a single catalyst pellet or substrate was placed in the coil region of our inductively-coupled RF plasma reactor, and a multi-substrate configuration. Our holistic approach to plasma diagnostics (i.e. determination of T_R and T_V and species densities and kinetic information) and comprehensive materials characterization enables us to more thoroughly investigate potential synergisms arising from the coupling of low temperature plasma and catalytic materials.

Experimental methods

All spectroscopic data were acquired in a glass tubular ICP reactor equipped with a multichannel spectrometer interfaced via a fiber optic cable, as described in detail previously, depicted in figure 1 [25]. For all experiments described herein, $P = 25$–150 W and $p = 50$–150 mTorr (6.7–20 Pa); the N_2 (Airgas, >99.99%) flow rate was ~3.5–10 sccm. For some experiments, a small amount of Ar (Airgas, >99.999%) was added to perform actinometric species density and T_e determination [26]. For steady-state emission experiments, integration times were 50 ms, with 100–150 averages; for time-resolved optical emission spectroscopy (TR-OES) collection parameters were 25 ms integration times with a single average. Emission from N_2 $C^3\Pi_u \rightarrow B^3\Pi_g$ (ν',ν'') [(0,0)] at 337.0 nm was monitored as a function of time and fit with a first order exponential to elucidate a rate constant of formation, denoted as k_f (s^{-1}), described previously [27]. In some experiments, a corresponding decrease in intensity to reach a steady state was observed and fit similarly, and here is denoted as a rate constant of destruction, k_d (s^{-1}). With a zeolite substrate, signals arising from NO $A^2\Sigma^+ \rightarrow X^2\Pi$ (0,1) at 235.9 nm and OH $A^2\Sigma^+ \rightarrow X^2\Pi$ (0,0) at 309.0 nm were observed (figure S2, see online supplementary information (stacks.iop.org/JPhysD/52/345202/mmedia)) and quantified to determine rate constants.

TiO_2 substrates were created from a slurry of as received TiO_2 AEROXIDE P25 nanopowder (Acros Organics, 21 nm primary particle size, specific surface area 35–65 $m^2\ g^{-1}$) and methanol applied to glass slides (VWR) or ~3 × 3 cm p-type ⟨1 0 0⟩ silicon wafers (Wacker-Chemitronic GMBH), as described previously [28, 29]. Glass slide substrates with TiO_2 were used in OES experiments and further characterized via XPS. Silicon wafers with TiO_2 were used for SEM analysis. The NaY zeolite substrates (Sigma Aldrich, 13×, 45/60 mesh molecular sieves) were ground with a mortar and pestle into a fine powder, 0.3 g of which was placed in an 18 000 psi pellet press (Carver) to create zeolite pellets with a 13 mm diameter and 2 mm height. The Brunauer–Emmett–Teller (BET) specific surface area of zeolites was determined by nitrogen

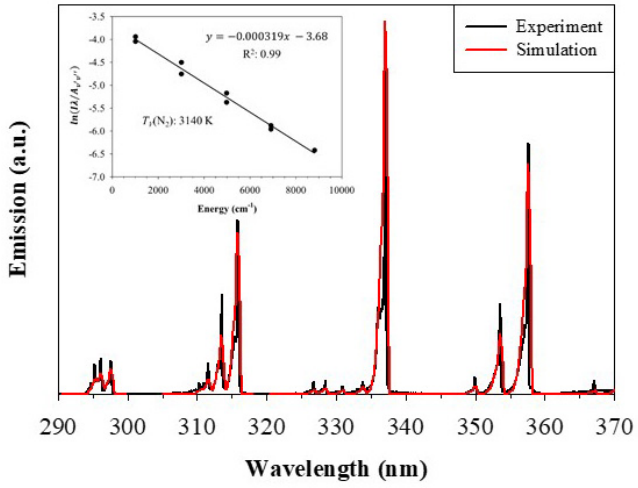

Figure 2. Representative emission spectrum at $p = 100$ mTorr, $P = 100$ W for N_2 ($C^3\Pi_u \rightarrow B^3\Pi_g$) in a N_2 plasma with TiO_2. Simulation of the spectrum using SpecAir yields $T_R = 350$ K. Inset shows a Boltzmann plot of N_2 vibrational distribution in a 100% N_2 plasma under the same conditions with a TiO_2 catalyst, calculated using the table 1 values.

adsorption curves (Micrometrics Analytical Service) due to the fabrication process of the as-received material. Specific surface area of the ground zeolite powder was measured as 930 m^2g^{-1}, more than an order of magnitude greater than that of the TiO_2 (see above). Substrates were placed directly in the coil region of the reactor, figure 1(a). Because of the small volume fraction of catalysts in this system (~0.1%), to examine the impact of the amount of catalyst present and to better compare to packed bed reactor literature results, the reactor was lined with zeolite pellets, figure 1(b), to create a multi-substrate reactor system, measuring energy partitioning and kinetic rate constants of relevant excited state species. In these studies, the zeolite pellets occupied ~2% of the plasma volume.

Powder x-ray diffraction (PXRD) data (Bruker D8 Discover DaVinci Powder x-ray Diffractometer, Cu K_α radiation source using 2θ from 5° to 80° at intervals of 0.02° with scans of 1 step s^{-1}) on the zeolite pellets were also collected (see figure S1), which demonstrate that N_2 plasma treatment does not appreciably change the crystallinity of the material. All substrates were further characterized using SEM (JEOL JSM-6500F with a field emission source; accelerating voltage of 15.0 kV; ~10 mm working distance) and XPS (PHI-5800 with a monochromatic Al K_α x-ray source (1486.6 eV photons)). CasaXPS v2.3 software was used to evaluate all high-resolution XPS spectra with Gaussian–Lorentzian (30:70) fits and peak FWHM were constrained to $\leqslant$2.0 eV. High-resolution C_{1s} spectra were charge corrected by setting the –C–C/–C–H component to 284.8 eV for all samples.

Results and discussion

As the table 1 data suggest, one of the key characteristics of N_2 plasmas is the internal temperatures of excited state N_2 in the plasma. As such, we first characterized our N_2 plasma without any substrates using OES. Figure 2 shows a typical N_2 emission spectrum acquired with a TiO_2 substrate placed in the coil region of the ICP. T_R (N_2) for the $C^3\Pi_u \rightarrow B^3\Pi_g$ transition was determined from simulated fits of experimental spectral data using SpecAir [30]. As described by Tu *et al* [20], a Boltzmann plot of ln ($I\lambda/A$) as a function of vibrational energy (E) was used to calculate T_V (N_2), where I and λ are the intensity (a.u.) and wavelength (nm) of a specific emission line and A (s^{-1}) is the corresponding Einstein transition probability coefficient for the transition. Table 2 lists the N_2 vibrational transitions, corresponding wavelengths, and A values used here [31, 32] and the inset in figure 2 shows a representative Boltzmann plot for a 100% N_2 plasma (with TiO_2 catalyst substrate) created from the corresponding spectrum and the table 2 data. The slope of the linear regression is inversely proportional to T_V, which ultimately yields $T_V = 3140 \pm 20$ K for the particular set of conditions shown in figure 2. A minimum of three trials were collected and fit for each condition reported. We previously reported T_V (N_2) values in N_2 plasmas [33]; however, these values were calculated using the 'Temperature Loop' function within SpecAir [30]. The simulation process within the SpecAir program uses Boltzmann distributions to determine vibrational temperatures, but does so while simultaneously considering electronic, rotational, and translational temperatures to achieve a best 'fit' to an experimental spectrum. It is not possible to simulate a spectrum with just vibrational temperature. Furthermore, the presence of zeolite substrates changes the corresponding emission spectrum, where there is clear overlap with the OH ($A^2\Sigma^+ \rightarrow X^2\Pi$) transition, figure S2. Therefore, fitting the entirety of the N_2 ($C^3\Pi_u \rightarrow B^3\Pi_g$ emission spectrum using SpecAir was challenging, whereas the table 2 spectral transitions utilized in the Boltzmann plot are independent of potential species (OH and NO) overlap. Thus, we believe the Boltzmann plot provides a more straightforward method to calculate T_V. In some cases, the previously reported values are within combined experimental error of those reported here. In those instances where the values differ appreciably, the methodology used herein results in higher T_V values than those acquired via the SpecAir simulation.

Table 2. Parameters for the vibrational bands in N_2 used to determine T_V (K) using a Boltzmann plot.

Vibrational transition	λ (nm)	$A_{v'\text{-}v''}$ (10^6 s^{-1})
$4 \rightarrow 2$	295.3	8.84
$3 \rightarrow 1$	262.2	6.61
$2 \rightarrow 0$	297.6	3.49
$3 \rightarrow 2$	311.6	5.48
$2 \rightarrow 1$	313.5	8.84
$1 \rightarrow 0$	315.9	10.2
$0 \rightarrow 0$	337.1	11
$1 \rightarrow 2$	353.6	4.61
$0 \rightarrow 1$	375.6	7.33

Figure 3 shows T_R and T_V data for N_2 with and without a TiO_2 substrate in a 100% N_2 plasma ($p = 13.3$ Pa (100 mTorr)) as a function of P. Numerical values for T_R and T_V measured

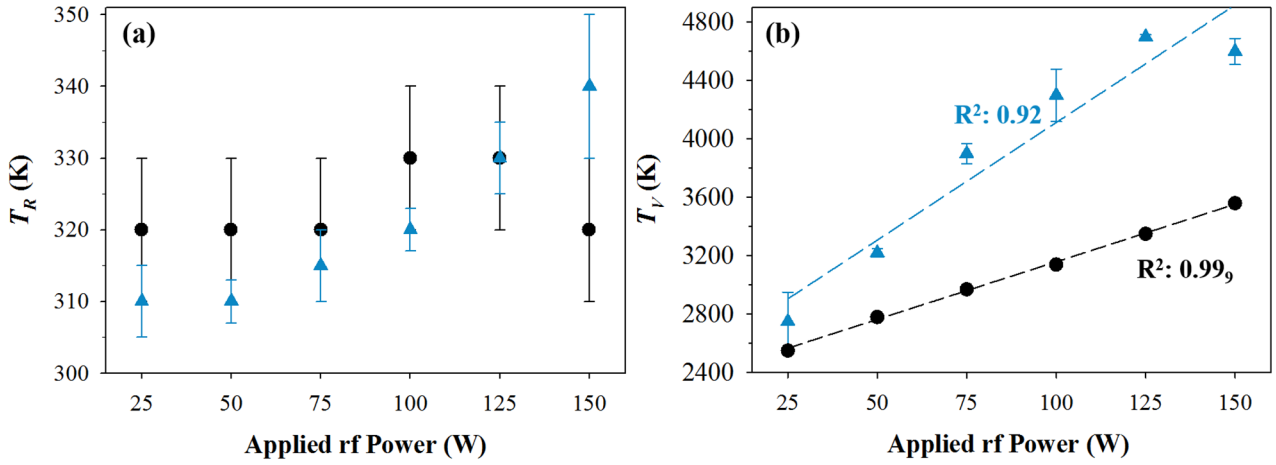

Figure 3. (a) T_R (N_2) and (b) T_V (N_2) from a N_2 plasma system at $p = 100$ mTorr with (black circles) and without (blue triangles) a TiO_2 substrate. Values for T_R without a substrate were previously reported [33].

Table 3. N_2 T_R (K) values in N_2 plasma systems[a].

p (mTorr)	P (W)	No substrate	TiO_2	Zeolite
50	25	305 (5)	300 (10)	310 (10)
	50	320 (5)	300 (10)	310 (5)
	75	320 (10)	310 (10)	320 (10)
	100	350 (10)	320 (10)	335 (5)
	125	360 (10)	320 (10)	340 (5)
	150	355 (5)	370 (10)	355 (5)
100	25	310 (5)	320 (10)	310 (10)
	50	310 (3)	320 (10)	340 (20)
	75	315 (5)	320 (10)	360 (5)
	100	320 (3)	330 (10)	350 (10)
	125	330 (5)	330 (10)	330 (10)
	150	340 (10)	320 (10)	360 (10)
150	25	300 (5)	300 (10)	305 (5)
	50	305 (5)	300 (10)	320 (10)
	75	—	330 (10)	320 (5)
	100	310 (5)	330 (10)	340 (14)
	125	—	330 (10)	350 (20)
	150	320 (5)	340 (10)	350 (10)

[a] Values in parentheses represent standard deviation calculated from the mean of $n \geqslant 3$ trials.

Table 4. $T_V(N_2)$ values in N_2 plasma systems[a].

p (mTorr)	P (W)	No substrate	TiO_2	Zeolite
50	25	2910 (90)	2310 (20)	2670 (100)
	50	4080 (70)	2560 (10)	3050 (90)
	75	3780 (50)	2780 (10)	3270 (100)
	100	4750 80)	3120 (120)	3800 (190)
	125	5560 (20)	3700 (270)	4230 (130)
	150	7000 (70)	4620 (70)	5070 (200)
100	25	2750 (200)	2550 (10)	2690 (190)
	50	3220 (30)	2780 (10)	3300 (40)
	75	3900 (70)	2970 (20)	3550 (50)
	100	4300 (180)	3140 (20)	3640 (120)
	125	4700 (15)	3350 (10)	3860 (200)
	150	4600 (90)	3560 (20)	3760 (200)
150	25	3320 (160)	2520 (20)	2990 (180)
	50	4470 (70)	2770 (10)	3530 (20)
	75	—	3010 (10)	3870 (30)
	100	5230 (140)	3150 (10)	4250 (40)
	125	—	3310 (20)	4500 (100)
	150	6020 (20)	3480 (10)	4980 (40)

[a] Values in parentheses represent standard deviation calculated from the mean of $n \geqslant 3$ trials.

under all conditions studied here are listed in tables 3 and 4, respectively. The T_R (N_2) data in the 100% N_2 plasma (no substrate), reported previously [33], show a small, but fairly linear increase with increasing P, with values near room temperature (~310–340 K), figure 3(a). Addition of a TiO_2 substrate does not appreciably change the overall values, but the P dependence has largely disappeared, within experimental error. In contrast, the T_V values shown in figure 3(b) show a strong linear dependence on P, both with and without the TiO_2 catalyst in the plasma. Interestingly, with the catalyst, the measured temperatures decrease by ~400–1000 K and the dependence on P decreases by approximately a factor of 2. This decrease in T_V (N_2) was documented at all pressures studied herein (50–150 mTorr), table 4. Notably, T_V (N_2) reaches values nearly an order of magnitude higher than T_R (N_2), suggesting that rotational relaxation is more efficient than vibrational relaxation. Within N_2 plasmas containing a TiO_2 substrate, as p increases from 50 mTorr (6.7 Pa) to 150 mTorr (20 Pa), some interesting trends emerge. At lower P (25–75 W), T_V (N_2) at 100 and 150 mTorr are within experimental error but are elevated compared to the 50 mTorr data. At higher P, as pressure is increased to 150 mTorr, there is significant quenching of the vibrational excited states, resulting in a decrease in T_V as a function of p.

Our results clearly demonstrate the presence of a TiO_2 catalyst within the plasma can dramatically impact T_V and agree to a certain extent with the results reported by Tu *et al* for a TiO_2 packed DBD system [20]. Overall, the actual values measured are similar to the literature work, with T_R slightly higher than room temperature (~300–600 K) and T_V significantly higher at ~2500–4500 K in both systems. In the DBD, however, the dependence of T_V on discharge power and catalyst display the

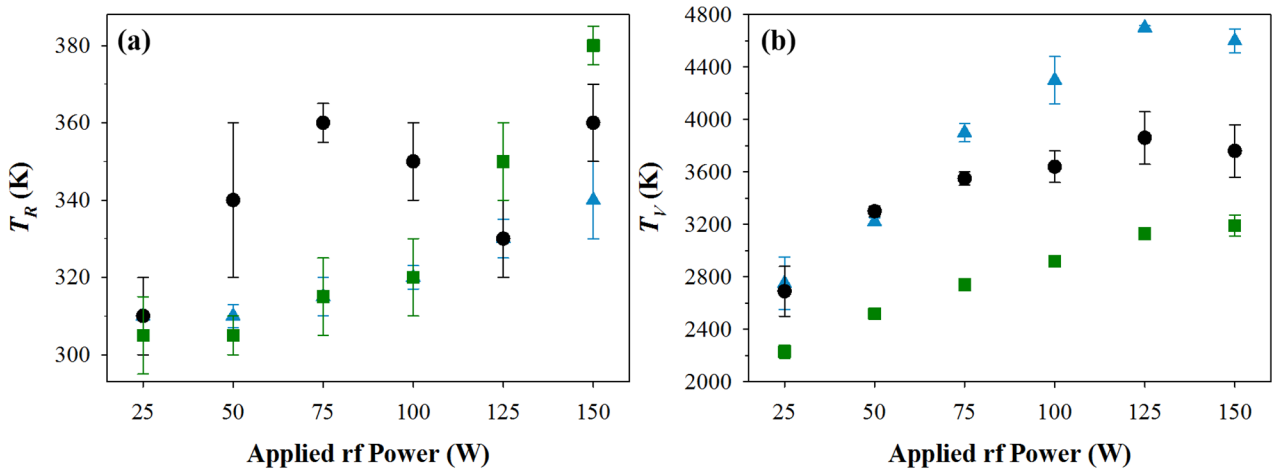

Figure 4. (a) T_R (N_2) and (b) T_V (N_2) from a N_2 plasma system at $p = 100$ mTorr without a catalyst (blue triangles); with a single zeolite pellet (black circles); and with multiple substrates (green squares). Values for T_R without a substrate were previously reported [33].

opposite behavior to that observed here: namely T_V decreases with P and significantly increases in the presence of the packed TiO_2. Notably, this P dependence previously observed was attributed to greater vibrational-translational relaxation at higher P, and the increase with the catalyst was attributed to an enhancement of the average electron energy in the plasma [20].

Possible explanations for these different trends lie primarily with the differences in the two plasma systems. Generally, emission intensity within a plasma is influenced by a number of factors, including electron energy distribution function (EEDF), direct or dissociative excitation, cascade processes, radiation transport, as well as elastic and inelastic collisions [34]. First, the DBD system operates at atmospheric pressure, whereas our systems operate at much lower pressures, thereby increasing the mean free path in the system. At atmospheric pressure, electronic quenching (the process by which a collision with species M removes energy from excited state species towards any other final product [35]) determines the lifetime of the excited electronic state, occurring on a longer timescale compared to radiative decay. As such, fewer collisions are likely to occur in our systems than in the DBD. Upon the addition of a substrate, there is greater likelihood of productive plasma-surface collisions, effectively quenching the N_2 excited states. Furthermore, plasma processing time is an important consideration, as the DBD system studied by Tu *et al* operated on the μs time scale [20], whereas our temperature studies investigate steady-state emissions from N_2 molecules on the timescale of minutes. Arguably, there can be vast differences in long-lived and short-lived species within plasma discharges [36], therefore future studies probing plasma internal temperatures as a function of time may be useful to understanding species' evolution during plasma processing.

Second, the catalyst in our system occupies only a small fraction of the total plasma volume, whereas Tu *et al*'s reactor is completely packed with TiO_2 nanoparticles. Thus, the surface area of catalyst available for interaction with the plasma is much larger in the Tu system. Moreover, the packed reactor reduces the plasma volume and gives rise to changes in the discharge mode which could promote decomposition or non-uniform electric fields in the system [2]. If the hypothesis that the catalyst enhances the average electron energy in the plasma is true, then this enhancement could be dependent on the amount of catalyst present. We have used the OES spectra acquired in our system to measure the T_e in our plasmas. We previously reported T_e for a 100% N_2 plasma (no substrate) and found $T_e \sim 1.6$ eV, regardless of P, [33]. Here, we found $T_e \sim 1.8$ eV for the same system with a TiO_2 substrate, also independent of P at $p = 50$ and 100 mTorr. The lack of significant dependence on P suggests increasing the overall energy of the system preferentially results in increasing the internal energy of neutrals or positive ions, rather than heating the electrons. Nevertheless, T_e appears to be slightly elevated in the presence of the TiO_2 catalytic material, indicating this catalyst does indeed slightly enhance the average T_e in our systems.

Exploring the impact of TiO_2 photocatalysts on the energy partitioning of N_2 plasmas allowed for a direct comparison to the work by Tu *et al* [20]. To further explore this work, we have also examined the impact of a different catalytic material on the gas-phase chemistry of an N_2 plasma. Figure 4 shows T_R (N_2) and T_V (N_2) as a function of P with and without a zeolite pellet in a 100% N_2 plasma. Although not nearly as dramatic as with TiO_2, a single zeolite pellet also decreases T_V (N_2), especially at the highest P, figure 4(b). The behavior for T_R (N_2) is much more complex. At the lower P (i.e. 50–100 W), T_R (N_2) with the zeolite pellet is higher than that measured in the system without the catalyst, figure 4(a). At $P \geqslant 125$ W, however, the values are the same within experimental error. Note, however, that T_R (N_2) values lie between 310 and 380 K, regardless of plasma conditions. Thus, these subtle fluctuations in values suggest T_R is relatively independent of system P, where rotational relaxation processes are less prominent in the presence of either catalyst. As noted above, a single catalyst in the coil region of the ICP reactor makes up a small fraction of the plasma volume; thus, a multiple zeolite substrate system (figure 1(b)) was also examined. As shown in figure 4(a), at $P \leqslant 125$ W, the addition of more zeolite catalysts to the N_2 discharge does not appreciably affect rotational cooling pathways. At $P = 150$ W, T_R (N_2) in the multiple substrate system is somewhat elevated compared to the other

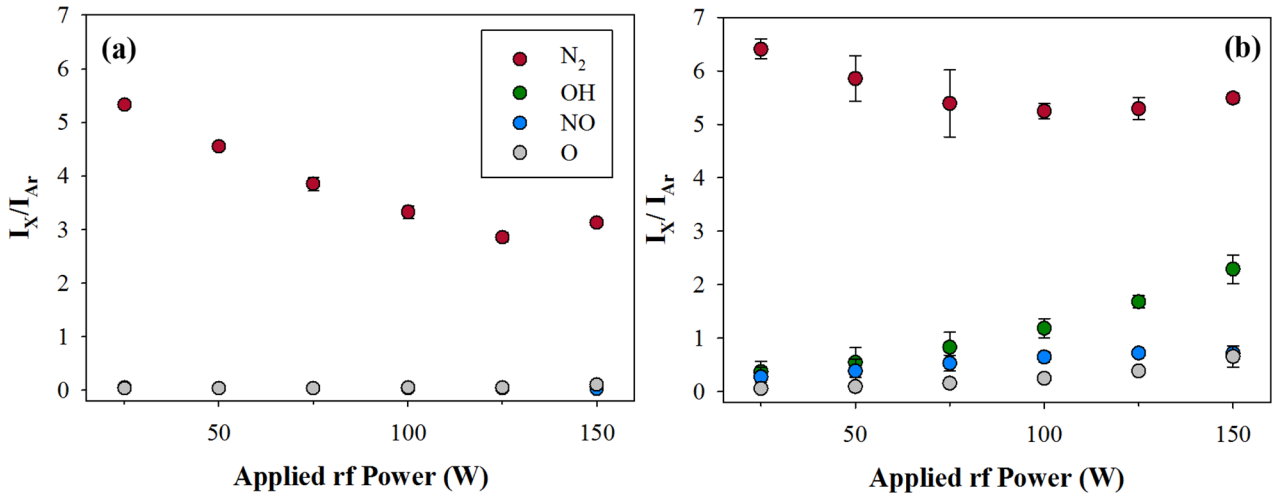

Figure 5. Relative species density as a function of applied RF power in a 100 mTorr N_2 plasma system without (a) and with a single (b) zeolite substrate.

systems. The plasma discharge switches between operating in E and H mode between 125 and 150 W, such that at 150 W the plasma is operating in H mode. Consequently, the change in T_R is likely a result of this mode shift. Catalyst packing can change the plasma operating mode, which has been studied experimentally and theoretically in DBD systems [37, 38]. Tu *et al* reported packing their entire reactor altered the discharge mode [9]. Thus, we hypothesize that as our ICP reactor became more 'packed' with zeolite catalysts, the accompanying mode shift may impact rotational energy distributions. Depicted in figure 4(b), the decrease in vibrational temperature observed with one pellet becomes more pronounced in the presence of multiple zeolite substrates. Vibrationally excited N_2 molecules clearly interact with the zeolite catalyst surface and can scatter with some energy loss; hence a decrease in vibrational energy is observed when a single zeolite pellet is present, and a larger decrease is documented in the multiple substrate system. These interactions can be explained through reaction (1),

$$N_{2(g)}\,(v') \rightarrow N_{2(ads)}\,(v') \rightarrow N_{2(g)}\,(v'') \qquad (1)$$

where v' and v'' indicate two different vibrational states, with v'' having a lower vibrational energy.

As shown in figure 5, inert gas actinometry was used to determine relative species' density as a function of P without and with a single zeolite substrate in the coil region, wherein molecular emissions from N_2 (337.0 nm), NO (235.9 nm), OH (309.0 nm) and atomic emission from O (777.2 nm) were monitored. Without a substrate, the amount of N_2 in the discharge decreases with increasing P, where there is little to no observable emissions from NO, OH, or O. N_2 emission displays a similar P dependence with a zeolite pellet in the plasma; however, the amount of NO, OH, and O all increase with increasing P in the catalyst loaded system. The increase in the oxygen-containing gas-phase species likely arise from the plasma interacting with SiO_2-rich zeolite, resulting in removal of surface oxygen. This decrease in T_V (K) in the presence of either catalyst suggest that within these low pressure discharges, vibrationally excited molecules interact with the substrates and rebound with some energy loss, hence a lower T_V (K) is measured [39]. Evaluating steady-state emission spectroscopy provides valuable information regarding energy distributions and relative species densities; however, it is also essential to utilize temporally-resolved data to probe the entangled dynamics in PAC relevant systems [40].

As shown in figure 6, intensity arising from N_2 emission at 337.0 nm was monitored as a function of time, where rate constants of formation (k_f) and destruction (k_d) were determined by fitting the intensity curve with first order exponentials (e^{-kt}). As evidenced in figure 6(a), the system with no substrate reached a steady state with no subsequent decay, hence a k_d is not reported. The addition of a zeolite catalysts significantly impacts the gas-phase chemistry, where a clear N_2 decay is documented. To further assess the dynamics within these systems, TR-OES was collected as a function of P, in the presence of single and multiple zeolite substrates (figure 7 and tables 5 and 6). Without a catalyst present, k_f values decrease as a function of P. Upon addition of the catalyst substrates to the system, interesting trends emerge. In the single zeolite system, rate constants increase from $P = 25$–75 W, then a corresponding decrease occurs as P is increased to 150 W. Although the rate constants for the multi-substrate reactor are significantly higher at $P = 50$–125 W, all three systems are within experimental error at 150 W. As noted above, the discharge is operating at H-mode under these conditions, suggesting the catalysts have a greater impact on reaction kinetics when the plasma is operating in E-mode.

Table 5 documents k_f for N_2, OH, and NO molecules in an N_2 plasma. There is little to no emission arising from NO or OH species in the system without a catalyst (figure 5), hence we cannot report kinetic data for these species in that system. At lower P in the single zeolite system (i.e. 25–75 W), we observe small signals attributable to NO (235.9 nm) and OH (309.0 nm) emission; however, rate constants could not be quantified from these data. Upon addition of more catalysts in the reactor, signal intensities increases and as such, rate constants were determined at lower powers, suggesting that the interactions occurring at the surface of a single catalyst are further enhanced upon additional of more surface

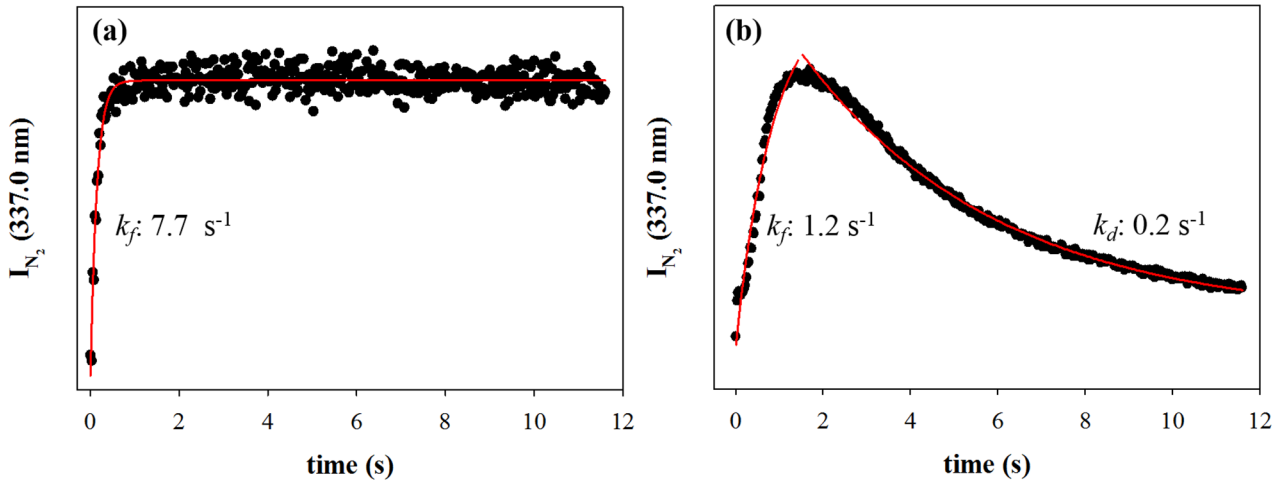

Figure 6. Intensity of N_2 emission plotted as a function of time at (a) $p = 100$ mTorr; $P = 50$ W with no substrate present; and (b) $p = 100$ mTorr; $P = 150$ W with a single zeolite pellet. Rate constants of formation and destruction were determined by fitting a first order exponential to each portion of the curve. Y axes are intensities in arbitrary units.

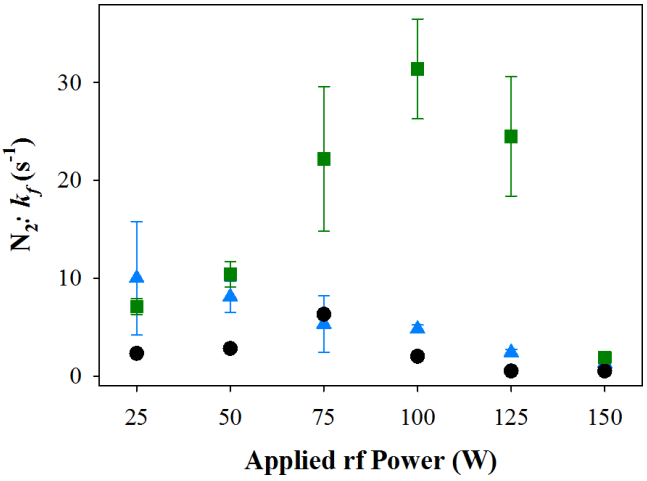

Figure 7. N_2 k_f (s^{-1}) from a N_2 plasma system at $p = 100$ mTorr without a catalyst (blue triangles); with a single zeolite pellet (black circles); and with multiple substrates (green squares).

area. The determined rate constants are, however, largely unaffected by the amount of catalyst in the system. Table 6 details k_d in the N_2 plasma with catalysts. Notably, a decay to steady-state emission is nominally only documented at higher *P.* Mehta *et al* argue the gas-phase is heavily influenced by active nitrogen species (i.e. N, N_2^+, and vibrationally excited N_2) and increased reaction rates in the presence of catalysts arise from N_2 molecules in low vibrational states on the surface [37]. For the multi-substrate system, at $P = 75$–125 W (figures 4 and 7), a clear enhancement in formation of excited N_2 molecules occurs, with a concomitantly lower T_V (i.e. less vibrationally active). Notably, these data were collected at intervals of 25 ms, a relatively long collection time. As such, it would be beneficial to obtain temporally resolved spectra on the μs scale to gain additional insight into the reaction kinetics in these systems. Nevertheless, the plasma gas-phase composition and the surface chemistry of the catalyst clearly have a measurable impact on the underlying kinetics in the system.

Table 5. k_f (s^{-1}) values in N_2 plasma systems with and without zeolite substrates[a,b].

k_f (s^{-1})	P (W)	No substrate	Single substrate	Multi-substrate
N_2	25	10.0 (5.8)	6.6 (2.3)	7.1 (0.8)
	50	8.1 (1.6)	11.1 (2.8)	10.4 (1.3)
	75	5.3 (2.9)	22.6 (6.3)	22.2 (7.4)
	100	4.8 (0.4)	15.3 (2.0	31.4 (5.1)
	125	2.4 (0.3)	3.6 (0.5)	24.5 (6.1)
	150	1.3 (0.06)	1.6 (0.5)	1.9 (0.5)
OH	25	NA	—	9.3 (2.5)
	50		—	11.0 (5.4)
	75		—	9.6 (1.9)
	100		4.4 (0.4)	3.6 (0.8)
	125		3.4 (0.5)	3.7 (0.6)
	150		1.1 (0.2)	2.1 (0.3)
NO	25	NA	—	—
	50		—	10.0 (1.9)
	75		—	8.7 (4.0)
	100		9.2 (1.4)	9.6 (5.1)
	125		3.9 (0.5)	5.6 (0.3)
	150		1.7 (0.5)	2.8 (0.5)

[a] Values in parentheses represent standard deviation calculated from the mean of $n \geqslant 3$ trials.
[b] '—' represents emission peaks were present, but could not be quantified.

Table 6. k_d (s^{-1}) values in N_2 plasma systems with zeolite substrates[a].

k_f (s^{-1})	P (W)	Single substrate	Multi-substrate
N_2	75	—	0.0092 (0.00014)
	100	—	0.013 (0.0051)
	125	0.055 (0.028)	0.019 (0.0088)
	150	0.16 (0.085)	0.054 (0.013)
OH	125	—	0.028 (0.00085)
	150	0.053 (0.027)	0.038 (0.0012)

[a] Values in parentheses represent standard deviation calculated from the mean of $n \geqslant 3$ trials.

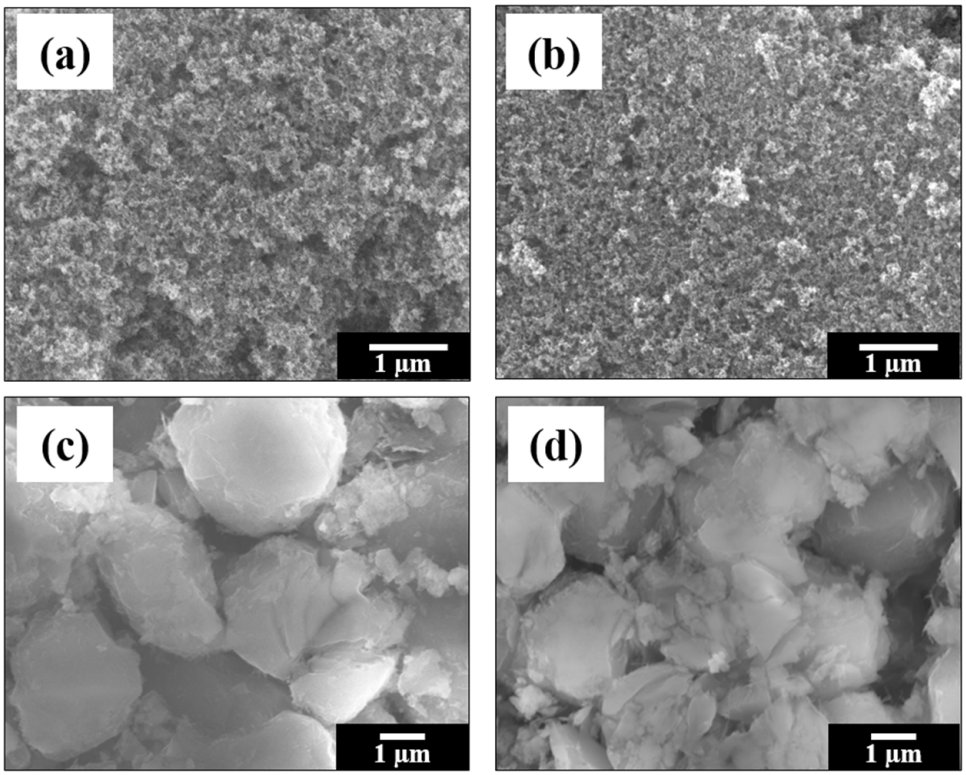

Figure 8. Representative SEM images (×20 000) of TiO_2 catalyst (a) as prepared on Si wafer substrate; (b) post N_2 plasma exposure and SEM images (×7000) of zeolite pellet (c) as prepared; and (d) post N_2 plasma exposure. Plasma exposure conditions for (b) and (c) were $P = 150$ W, $p = 100$ mTorr, $t = 10$ min.

As noted in the Introduction, we sought to examine how the presence of a catalyst impacts the energetics within the discharge using both micro- and nano-structured materials. When comparing T_V (N_2) in the systems with a catalyst, the vibrational temperatures documented with a zeolite pellet present are elevated relative to those in the TiO_2 system under all experimental conditions, table 4. Factors to consider when comparing the two substrates include size and geometry of pores, as well as chemical properties. With a 2D fluid model, Zhang *et al* demonstrated that the shape of a catalyst pore has significant impact on the electric field within a plasma, thus substantial impact on the resulting plasma properties [41]. Their results indicated that the electric field enhancement was largest for conical pores, and that those with small openings experienced a large increase in ionization rate relative to those with larger openings. In our systems, the pores in the TiO_2 substrates have significantly smaller openings than those in the zeolite pellets, suggesting plasma generation near and in the pores of the TiO_2 may be heightened, ultimately leading to more vibrational quenching interactions with the catalyst surface. As TiO_2 is also a known photocatalyst, the UV light generated from the plasma may further active these materials and contribute to additional vibrational quenching of the N_2 ($C^3\Pi_u$) state. Nasonova and Kim coated zeolite materials with TiO_2 particles to observe possible synergisms upon coupling a catalyst with a photocatalyst for NO and SO_2 removal [42]. The authors demonstrated these hybrid materials increased both NO and SO_2 removal efficiencies [42]; however, they did not characterize plasma internal temperatures. As TiO_2 nanoparticles supported on glass substrates have a large impact on T_V (N_2) within our low-temperature RF discharges, a logical step forward would be to assess the impact on TiO_2 particles supported on materials with larger surface areas. Regardless of the pore size or surface area of a specific catalyst, clearly addition of a catalyst alters the gas-phase plasma chemistry. Consequently, we also examined how the catalysts were changed through gas-surface interactions in the plasma.

N_2 plasmas have been used to create metal nitrides and other materials and nitrogen is known to readily replace oxygen in metal oxide lattices [43, 44]. We have explored the morphology and surface composition of the two catalysts before and after exposure to N_2 plasmas using SEM and XPS. The commercially purchased TiO_2 material agglomerates into nanoparticle clusters with a porous structure when pasted onto the glass substrate [28], figure 8(a). This morphology does not change appreciably upon exposure to the N_2 plasma, figure 8(b), regardless of P or p over the parameter space explored herein. Likewise, the morphology of the zeolite pellet does not change appreciably upon plasma treatment, figures 8(c) and (d). The SEM images shown in figure 8 also highlight the size disparity between the nano-structured TiO_2 and micro-structured zeolite. As described in the Introduction, a goal of this work was to investigate the impact of materials (both nano- and micro-structured) on gas-phase composition and energetics, as well as assess material properties post plasma exposure.

Figure 9 contains high-resolution O_{1s} and Ti_{2p} spectra for TiO_2 prior to and post N_2 plasma exposure ($p = 100$ mTorr,

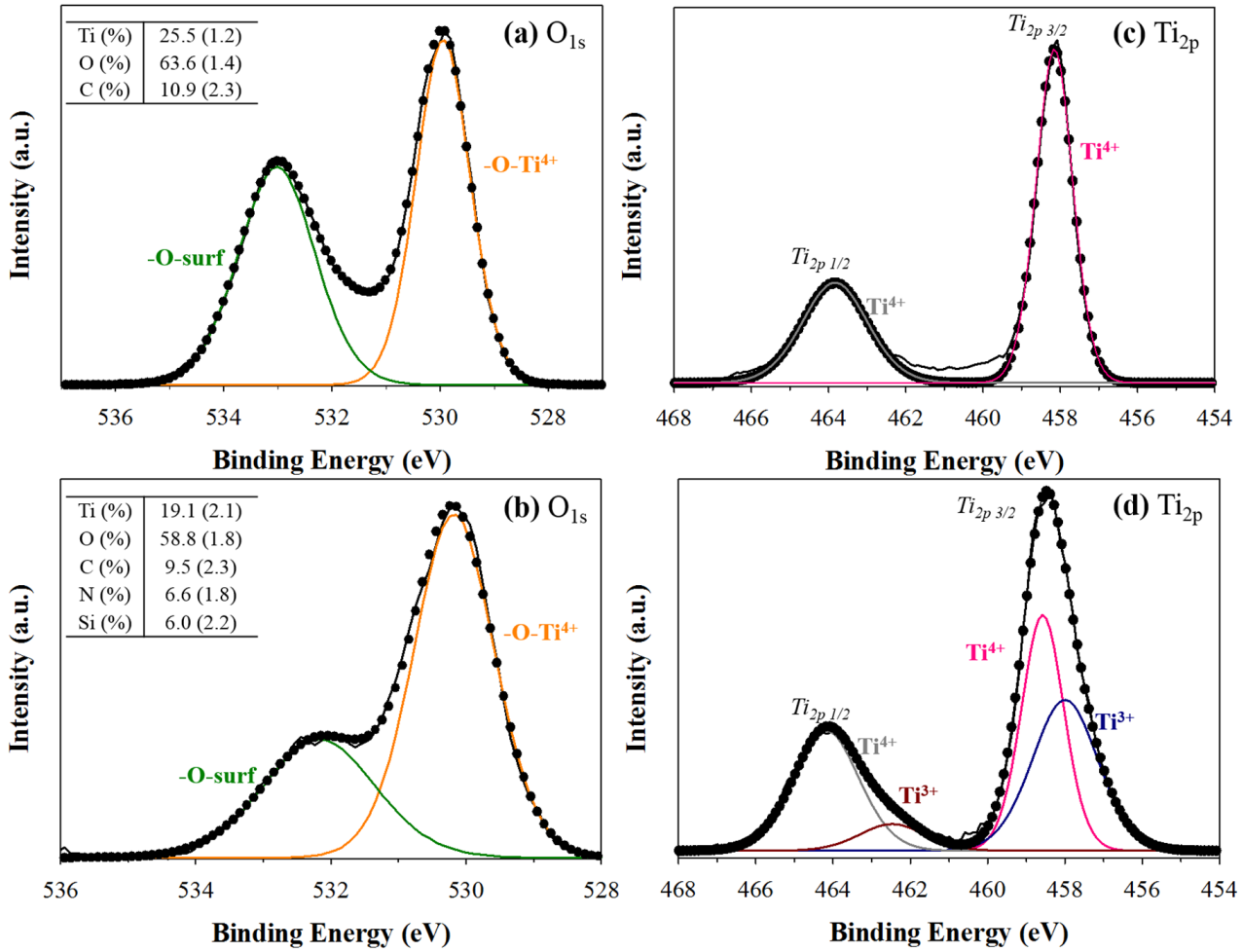

Figure 9. XPS high resolution O_{1s} and Ti_{2p} data for TiO_2 prior to plasma exposure (a) and (c) and after N_2 plasma ($p = 100$ mTorr, $P = 150$ W, $t = 10$ min) exposure (b) and (d), respectively. Inset tables report atomic composition data.

$P = 150$ W, $t = 10$ min). The primary contribution to the O_{1s} spectra in untreated TiO_2 arises, as expected, from oxygen bound to Ti^{4+} (530.2 eV) [18], figure 9(a), with a smaller peak assigned to oxygen adsorbed to the material surface, such as hydroxyl species (532.1 eV) [18, 45]. An increase of adsorbed surface oxygen post N_2 plasma processing, figure 9(b), is likely the result of the plasma creating oxygen vacancies within the TiO_2 lattice, which ultimately decreases the relative contribution of the bound oxygen [18, 19]. High resolution Ti_{2p} spectra of the untreated TiO_2 material, figure 9(c), show binding energies for $Ti_{2p3/2}$ and $Ti_{2p1/2}$ at 458.6 eV and 464.2 eV, respectively, corresponding to surface titanium in the Ti^{4+} oxidation state [18]. Additional binding environments at 457.9 eV and 462.5 eV corresponding to Ti^{3+} exist in the spectrum of the TiO_2 substrates post N_2 plasma exposure, figure 9(d), suggesting nitrogen doping [18, 44]. Specifically, the formation of a O–Ti–N binding environment by substitution of an O atom in the TiO_2 lattice with a N atom is attributed to a shift toward lower binding energy [46]. High-resolution C_{1s} spectra, figure S3, show binding environments for –C–C/–C–H (284.8 eV), –C–O–R/–C–O–H (286.3 eV), and –C=O (288.7 eV) for the TiO_2 substrate before and after plasma treatment. From these spectra and the corresponding inset tables of elemental composition, figures 9(a) and (b), exposure to the N_2 plasma does not appear to significantly change the nature or amount of carbon on the TiO_2 nanoparticle surface. We do, however, observe a small, but non-negligible amount of nitrogen incorporated into the TiO_2 catalyst surface. Similarly, Lu *et al* utilized Fourier transform infrared (FTIR) spectroscopy and XPS spectra to document nitrogen doping into the structure of the TiO_2 coated dielectric of their parallel-plate DBD reactor [46]. Pulsipher *et al* also observed nitrogen incorporation into TiO_2 substrates upon exposure to a range of nitrogen-containing plasmas, including N_2-based systems [29].

Table 7. XPS atomic composition data for zeolite pellets[a,b].

	Untreated	125 W	150 W	175 W
Si (%)	15.5 (2.6)	23.1 (2.9)	18.7 (5.2)	21.0 (0.5)
O (%)	57.5 (4.0)	59.7 (3.5)	56.4 (5.3)	53.1 (0.5)
Al (%	4.4 (0.6)	6.8 (0.7)	13.1 (7.7)	4.3 (0.3)
C (%)	22.7 (7.0)	10.5 (6.0)	11.8 (3.0)	14.1 (1.0)
N (%)	—	—	—	7.4 (0.3)

[a] Values in parentheses represent one standard deviation for the measurement.
[b] Treatment conditions: $p = 100$ mTorr, $t = 10$ min.

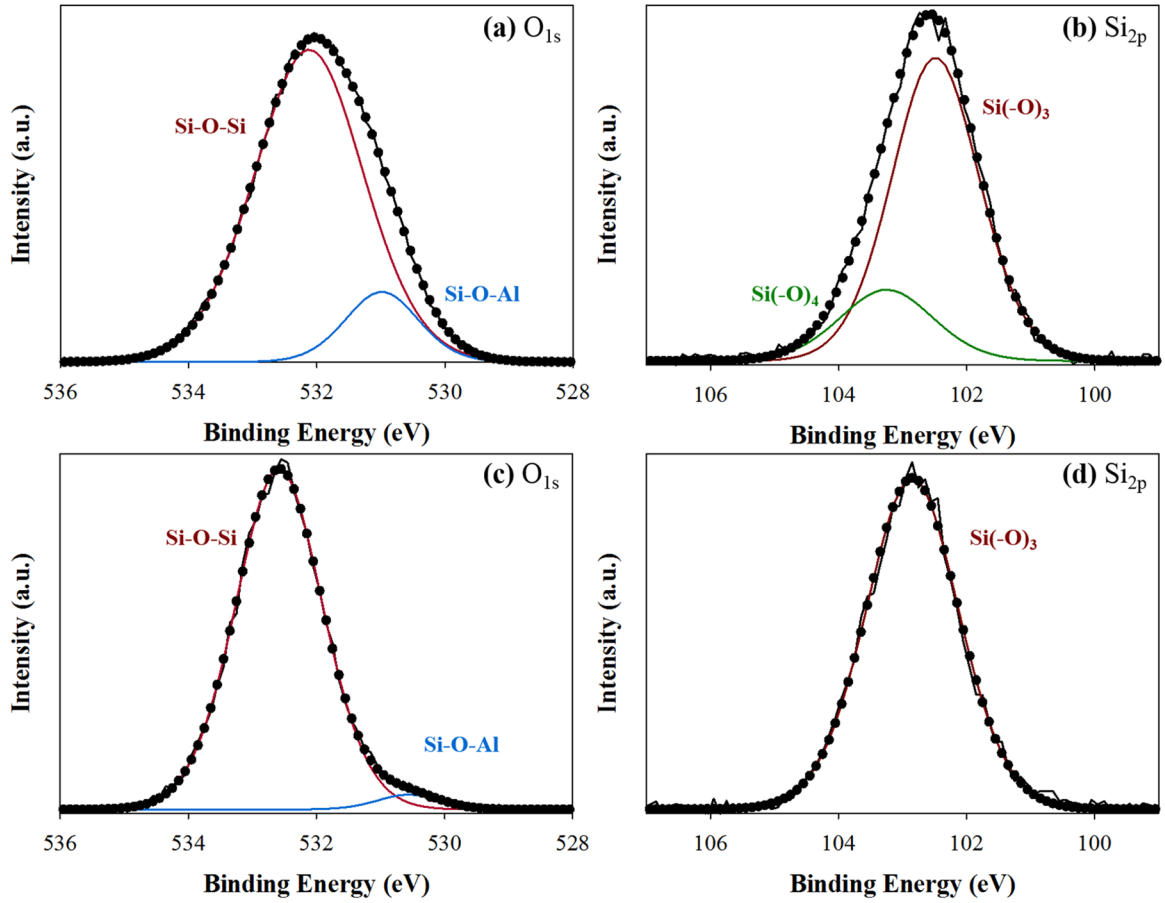

Figure 10. XPS high resolution O_{1s} and Si_{2p} data for zeolite pellets prior to plasma exposure (a) and (b) and after N_2 plasma ($p = 100$ mTorr, $P = 150$ W, $t = 10$ min) exposure (c) and (d).

Compositional data from high-resolution XPS spectra, table 7, reveal untreated zeolite pellets, are nominally composed of Si, O, and Al, with ~23% C bound in environments corresponding to –C–C/–C–H, –C–O–R/–C–O–H, and –C=O (figures 10 and S3). As shown in SEM images, figure 8, zeolites are porous materials with a high surface area, therefore the adsorption of large amounts of atmospheric (adventitious) carbon is expected on the surface. High-resolution O_{1s} and Si_{2p} spectra, figure 10, further corroborate this evidence, as the primary oxygen binding environments include the Si–O–Si band at 531.7 eV and the Si–O–Al band at 530.8 eV [47, 48]. Oxygen adsorbed to the material or bound to adventitious carbon can be present at binding energies 532.6–532.1 eV, which is difficult to deconvolute from the Si–O–Si band. High-resolution Si_{2p} data, figures 10(b) and (d), show two Si binding environments, Si(–O_4) at 103.4 eV and Si(–O_3) at 102.8 eV [49], corresponding to an inorganic SiO_2 network, which nominally changes to a single binding environment at 102.8 eV post N_2 plasma treatment, figure 10(d). For PAC to be a viable and usable technology, these catalysts must be robust and able to withstand intense plasma exposure. Table 7 documents elemental composition of zeolite pellets post N_2 plasma exposure at a range of P. At 125 and 150 W, there are little to no changes in elemental composition, within error, except for the Al. At both P, the percent of Al slightly increases from the untreated, suggesting removal of adventitious carbon and oxygen from the surface. This is further substantiated by the gas-phase chemistry and SEM, where an increase in NO, OH, and O is documented (figure 5(b)). In figure 8(d), there appears to be areas of the zeolite that have been etched (or pitted), likely disrupting the zeolite Si–O–Si and Si–O–Al bonding bridges. At $P = 175$ W, the most intense plasma conditions studied herein, the XPS data show significant nitrogen incorporation into the surface of the material. Furthermore, the O_{1s} and Si_{2p} binding environments are largely unchanged compared to the untreated material (figures 10(a) and (c)), as well as the morphology (figures 8, and S4) and overall bulk crystallinity of the material (figure S1), suggesting these materials still retain the properties that make them desirable catalysts.

The gas-surface interactions studied herein are schematically depicted in figure 11. Although numerous possible gas-catalyst interactions exist, we believe these four are the most prevalent in our systems. XPS data reveal that under certain operating conditions, N is doped into both the zeolite and TiO_2 substrates. The etching of lattice oxygen in both TiO_2 and zeolite (nominally SiO_2) substrates can occur when excited state nitrogen impinges and reactors to form additional gas-phase species (i.e. NO, OH) as depicted in figure S1 and reaction (2),

$$N_2^*(g) + 2O(g) \rightarrow 2NO^*(g) \quad (2)$$

where N_2^* and NO^* represent excited state species. Ultimately, we believe there is still much work to be done to further

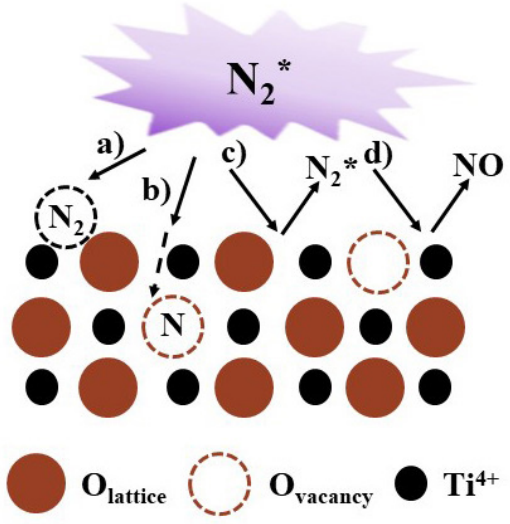

Figure 11. Schematic representation of selected surface modification processes occurring during N_2 plasma processing: (a) surface adsorption; (b) N-doping of the substrate; (c) energetic bombardment resulting in vibrational quenching; (d) etching and formation of new gaseous species such as NO.

understand the underlying mechanisms involved in PAC systems. Nevertheless, the data presented herein clearly demonstrate that not only does the plasma alter the surface of catalytic substrates, but the presence of both micro- and nano-structured catalytic materials clearly alter energy partitioning within the gas-phase of the plasma.

Summary

As evidenced by gas-phase energetics data and resulting materials characterization, there is a synergistic, dynamic interface that arises when a plasma is coupled with catalysts. Regardless of material surface area, the presence of a catalyst in the coil region of a low-pressure RF plasma results in a pronounced decrease in the vibrational temperature of gas-phase species, with no clear or significant impact on rotational cooling pathways. For PAC to become a viable means of pollution control, it is essential that these energetic pathways and plasma-surface interactions be further examined. Notably, all work presented herein characterized excited state species; we have shown previously a significant energetic difference between ground and excited state N_2 and NO molecules [25, 33]. As such, additional data on ground-state molecules in the system could provide further insight into energy partitioning within these systems. Finally, employing our unique imaging radicals interacting with surfaces (IRIS) technique to determine a molecule's propensity to scatter from both nano- and micro-structured surfaces may provide more direct evidence of how plasma species synergistically interact with catalytic substrates. This holistic experimental approach, combining gas-phase diagnostics, IRIS, and robust materials characterization will be essential to realizing the potential of PAC for pollution remediation.

Acknowledgments

This work was supported by the National Science Foundation (NSF CBET—1803067). The authors would like to thank Professor Joseph A DiVerdi for providing assistance and expertise on our BET measurements and analysis; and the staff of the CSU Central Instrument Facility for assistance with the XPS, XRD, and SEM analyses.

ORCID iDs

Ellen R Fisher https://orcid.org/0000-0001-6828-8600

References

[1] Bacariza M C, Biset-Peiro M, Graca I, Guilera J, Morante J, Lopes J M, Andreu T and Henriques C 2018 *J. CO_2 Util.* **26** 202–11
[2] Feng X, Liu H, Hi C, Shen Z and Wang T 2018 *Catal. Sci. Technol.* **8** 936–54
[3] Puliyalil H, Jurkovic D L, Dasireddy V D B C and Likozar B 2018 *RSC Adv.* **8** 27481–508
[4] Neyts E C 2016 *Plasma Chem. Plasma Process* **36** 185–212
[5] Van Durme J, Dewulf J, Leys C and Van Langenhove H 2008 *Appl. Catal.* B **78** 324–33
[6] Xu W, Lin K, Ye D, Jiang X, Liu J and Chen Y 2019 *Nanomaterials* **9** 290
[7] Mei D, Zhu X, He Y-L, Yan J D and Tu X 2014 *Plasma Sources Sci. Technol.* **24** 015011
[8] Chen G, Britun N, Godfroid T, Georgieva V, Snyders R and Delplancke-Ogletree M-P 2017 *J. Phys. D: Appl. Phys.* **50** 084001
[9] Tu X and Whitehead J C 2012 *Appl. Catal.* B **125** 439–48
[10] Mustafa M F, Fu X, Liu Y, Abbas Y, Wang H and Lu W 2018 *J. Hazard. Mater.* **347** 317–24
[11] Peng P *et al* 2018 *J. Clean. Prod.* **177** 597–609
[12] Santhosh N M, Filipič G, Tatarova E, Baranov O, Kondo H, Sekine M, Hori M, Ostrikov K K and Cvelbar U 2018 *Micromachines* **9** 565
[13] Taghvaei H, Heravi M and Rahimpour M R 2017 *Plasma Process. Polym.* **14** 1600204
[14] Adamovich I *et al* 2017 *J. Phys. D: Appl. Phys.* **50** 323001
[15] Whitehead J C 2016 *J. Phys. D: Appl. Phys.* **49** 243001
[16] Malik M A, Minamitani Y and Schoenback K H 2005 *IEEE Trans. Plasma Sci.* **33** 50–6
[17] Gong X, Zhao R, Qin J, Wang H and Wang D 2019 *Chem. Eng. J.* **358** 291–8
[18] Wu H, Xu C, Xu J, Lu L, Fan Z, Chen X, Song Y and Li D 2013 *Nanotechnology* **24** 455401
[19] Han J-B, Wang X, Wang N, Wei Z-H, Yu G-P, Zhou Z-G and Wang Q-Q 2006 *Surf. Coat. Technol.* **200** 4876–8
[20] Tu X, Gallon J and Whitehead J C 2011 *J. Phys. D: Appl. Phys.* **44** 482003
[21] Niu J, Peng B, Yang Q, Cong Y, Liu D and Fan H 2013 *Cat. Today* **211** 58–65
[22] Tu X, Verheyde B, Cofrthais S, Paulussen S and Sels B F 2011 *Phys. Plasmas* **18** 080702
[23] Zhang Y, Wang H-Y, Zhang Y-R and Bogaerts A 2017 *Plasma Sources Sci. Technol.* **26** 054002
[24] Gu J-G, Zhang Y, Gao M-X, Wang H-Y, Zhang Q-Z, Yi L and Jiang W 2019 *J. Appl. Phys.* **125** 153303
[25] Blechle J M, Hanna A R and Fisher E R 2017 *Plasma Process. Polym.* 1700041

[26] Boogaard A, Kovalgin A Y, Aarnink A A I, Wolters R A M, Holleman J, Brunets I and Schmitz J 2006 Measurement of electron temperatures of argon plasmas in a high-density inductively-coupled remote plasma system by Langmuir probe and optical-emission spectroscopy *Proc. 9th Annual Workshop on Semiconductor Advances for Future Electronics and Sensors 2006* (Utrecht, The Netherlands: Technology Foundation STW) pp 412–8
[27] Cuddy M F and Fisher E R 2012 *ACS Appl. Mater. Interfaces* **4** 1733–41
[28] Shearer J C, Fisher M J, Hoogeland D and Fisher E R 2010 *Appl. Surf. Sci.* **256** 2081–91
[29] Pulsipher D J V, Martin I T and Fisher E R 2010 *ACS Appl. Mater. Interfaces* **2** 1743–53
[30] Laux C O 2002 Radiation and nonequilibrium collisional-radiative models *von Karman Institute Lecture Series, Physico-Chemical Modeling of High Enthalpy and Plasma Flows* ed D Fletcher *et al* (Rhode-Saint-Gense, Belgium)
[31] Wu A J, Zhang H, Li X D, Lu S Y, Du C M and Yan J H 2015 *IEEE Trans. Plasma Sci.* **43** 836–45
[32] NIST *NIST Chemistry WebBook* (http://webbook.nist.gov/chemistry) (Accessed: 12 October 2018)
[33] Hanna A R, Blechle J M and Fisher E R 2017 *J. Phys. Chem. A* **121** 7627–40
[34] Meichsner J, Schmidt M, Schneider R and Wagner H E 2012 *Nonthermal Plasma Chemistry and Physics* (London: Taylor and Francis)
[35] Dilecce G 2014 *Plasma Sources Sci. Technol.* **23** 015011
[36] Grill A 1994 *Cold Plasma Materials Fabrications: From Fundamentals to Applications* (Piscataway, NJ: IEEE)
[37] Mehta P, Barboun P, Go D B, Hicks J C and Schneider W F 2019 *ACS Energy Lett.* **4** 1115–33
[38] Wang W, Kim H-H, Van Laer K and Bogaerts A 2018 *Chem. Eng. J.* **334** 2467–79
[39] Hanna A R, Cuddy M F and Fisher E R 2017 *J. Vac. Sci. Technol. A* **35** 05C308
[40] Fridman A 2008 *Plasma Chemistry* (Cambridge: Cambridge University Press)
[41] Zhang Y-R, Neyts E C and Bogaerts A 2018 *Plasma Sources Sci. Technol.* **27** 055008
[42] Nasonova A and Kim K-S 2013 *Cat. Today* **211** 90–5
[43] Antonczak A J, Skowronski L, Trzcinski M, Kinzhybalo V V, Lazarek L K and Abramski K M 2015 *Appl. Surf. Sci.* **325** 217–26
[44] Kollbek K, Szkudlarek A, Marzec M M, Lyson-Sypien B, Cecot M, Bernasik A, Radecka M and Zakrzewska K 2016 *Appl. Surf. Sci.* **380** 73–82
[45] Cao Y, Meng Q, Yang W, Yao J, Shu Y, Wang W and Chen G 2005 *Colloids Surf. A* **262** 181–6
[46] Lu N, Hui Y, Shang K, Jiang N, Li J and Wu Y 2018 *Plasma Chem. Plasma Process.* **38** 1239–58
[47] Cui X, Chen C, Sun S, Zhou D, Ndayisenga F, Huo M, Zhu S, Zhang L and Crittenden J C 2018 *Water Res.* **143** 136–45
[48] Groening P and Biino G G 1998 *Eur. J. Mineral.* **10** 423–37
[49] Alexander M R, Short R D, Jones F R, Michaeli W and Blomfield C J 1999 *Appl. Surf. Sci.* **137** 179–83
[50] Porter R A and Harshbarger W R 1979 *J. Electrochem. Soc.* **126** 460–4
[51] Cernogora G, Ferreira C M, Hochard L, Touzeau M and Loureiro J 1984 *J. Phys. B: At. Mol. Phys.* **17** 4429–37
[52] Zhang J, Liu L, Ma T and Deng X 2002 *Spectrochim. Acta A* **58** 1915–22
[53] Masoud N, Martus K, Figus M and Becker K 2005 *Contrib. Plasma Phys.* **45** 32–9
[54] Britun N, Gaillard M, Ricard A, Kim Y M, Kim K S and Han J G 2007 *J. Phys. D: Appl. Phys.* **40** 1022–9
[55] Gangoli S P, Gutsol A F and Fridman A A 2010 *Plasma Sources Sci. Technol.* **19** 065003
[56] Yang F, Mu Z and Zhang J 2016 *Plasma Sci. Technol.* **18** 79–85
[57] Gröger S, Ramakers M, Hamme M, Medrano J A, Bibinov N, Gallucci F, Bogaerts A and Awakowicz P 2018 *J. Phys. D: Appl. Phys.* **52** 065201